

BOHMIAN MECHANICS APPLIED TO OPEN QUANTUM SYSTEMS

by

Ethan Keller

A thesis submitted to the faculty of  
The University of North Carolina at Charlotte  
in partial fulfillment of the requirements  
for the degree of Master of Science in  
Applied Physics

Charlotte

2024

Approved by:

---

Dr. Donald Jacobs

---

Dr. Greg Gbur

---

Dr. Xingjie Li



## ABSTRACT

ETHAN KELLER. Bohmian Mechanics Applied to Open Quantum Systems. (Under the direction of DR. DONALD JACOBS)

This thesis advances our understanding of quantum phases and their interplay with particle trajectories in closed and open Bohmian systems, employing the innovative Quantum Velocity Search Algorithm to reconstruct wave functions and perform bulk phase statistics. Analysis of closed systems reveals significant insights into velocity distributions and positional velocity constraints. In closed systems, the analysis uncovered that modulating the initial phase on the expansion coefficients for the energy eigenstates, as well as the number of terms in the expansion, significantly influences positional velocity characteristics. The number of terms restricts the maximum velocity that can be achieved. For example, 4 terms produce 1 Å/fs at the center of the box compared to 300 Å/fs with 18 terms. Many different sets of initial phase values can lead to the same velocity. Open systems are modeled by dynamically changing the phase factors as a stochastic process to model the influence of the environment. Examination of open systems highlights their disruptive effect on the quantum behavior for a closed system, with the phase diffusion coefficient being linked to rates of thermal energy transfer into and out of the system. The relationship between energy rates and phase coefficients creates a maximal energy rate because angle deviations repeat every  $2\pi$ . This research underscores the alternative perspectives between determinism in chaotic systems compared to a probabilistic interpretation in quantum mechanics, setting a foundation for future exploration of open quantum systems within the Bohmian framework.

## TABLE OF CONTENTS

|  |     |
|--|-----|
| LIST OF TABLES   | vi  |
| LIST OF FIGURES  | vii |
| CHAPTER 1: INTRODUCTION  | 1   |
| 1.1. Characterizing Bohmian Mechanics                              | 2   |
| 1.2. Defining Open/Closed Quantum Systems                          | 2   |
| 1.3. Characterizing Open Quantum Systems                           | 3   |
| 1.4. Current Methods of Computing Open Quantum Systems             | 4   |
| 1.4.1. Lindblad Model  | 4   |
| 1.4.2. Nakajima-Zwanzig Model                                      | 5   |
| 1.4.3. Caldeira-Leggett Model                                      | 5   |
| 1.4.4. Stochastic Bohmian Mechanics Models for Open Quantum System | 6   |
| 1.4.5. Modified Schrodinger Equation Approach                      | 8   |
| 1.5. Stationary States of Open Quantum Systems                     | 10  |
| 1.6. System of Interest: Particle in a Box                         | 10  |
| 1.6.1. Objectives of Study   | 12  |
| CHAPTER 2: METHODOLOGY   | 13  |
| 2.1. Diffusive Processes as Open Quantum System Perturbations      | 13  |
| 2.1.1. Magnitude and Number of Expansion Coefficients              | 15  |
| 2.2. Numerical Scheme for Particle Trajectories                    | 15  |
| 2.3. Quantum Velocity Search Algorithm                             | 16  |
| 2.4. Calculating Standard Deviation of Phase Sets                  | 16  |

|                                     |    |
|-------------------------------------|----|
|                                     | v  |
| CHAPTER 3: RESULTS                  | 18 |
| 3.1. Closed Systems                 | 18 |
| 3.1.1. Single Point Evaluation      | 19 |
| 3.1.2. Linear Evaluation            | 20 |
| 3.2. Open Systems                   | 24 |
| 3.2.1. Phase to Energy Relationship | 24 |
| 3.2.2. Trajectory Analysis          | 25 |
| CHAPTER 4: CONCLUSION               | 32 |
| REFERENCES                          | 33 |

## LIST OF TABLES

|  |    |
|--|----|
| TABLE 2.1: Table detailing a sample standard deviation calculation for phase sets. | 17 |
|--|----|

## LIST OF FIGURES

- FIGURE 1.1: Bohmian trajectories for Young's double slit experiment which produce the characteristic interference pattern centered at the midpoint of the two slits. Retrieved from page 57 of [1]. 1
- FIGURE 3.1: Frequency count of velocities generated as initial conditions with  $\sigma_\phi$  increasing in tenfold increments. Red represents negative velocity values, blue represents positive. The standard deviation of velocity is given in the top right of each graph. 20
- FIGURE 3.2: The mean of standard deviations as a function of  $\log_{10}$  of samples (left) shows each mean value with a small square box and vertical error bars. The mean of  $\log_{10}$  of kurtosis as a function of  $\log_{10}$  of samples (right) shows each mean value with a small square box and vertical error bars. 21
- FIGURE 3.3: Surface plots highlighting position and velocity as inputs for the search algorithm which outputs phases for box sizes of  $50\text{\AA}$  (left) and  $100\text{\AA}$  (right). The standard deviation of each set of phases are represented as colors along the grid. The color bar is a legend showing the range of values and the corresponding colors. 22
- FIGURE 3.4: Sets of 5 probability densities generated from initial conditions with box size of  $100\text{\AA}$  and search velocities of  $0.5\text{\AA}/\text{fs}$  (left) and  $5\text{\AA}/\text{fs}$  (right). 23
- FIGURE 3.5: Surface plot highlighting position and velocity as inputs for the search algorithm which outputs phases for a box size of  $200\text{\AA}$ . The standard deviation of each set of phases are represented as colors along the grid. The color bar is a legend showing the range of values and the corresponding colors. 23
- FIGURE 3.6: Average standard deviation of velocity as a function of standard deviation of phases (solid blue). A linear fit (black dashed line) with a slope of  $2\text{\AA}/(\text{fs rad})$  is fitted to the initial portion (approximately  $0.55\text{ rad}$ ) until saturation is met, represented by the median value of  $1.134\text{\AA}/\text{fs}$  (red dashed line). 24
- FIGURE 3.7: Log-Log plot of Energy Rate as a function of standard deviation of phase (solid black). The horizontal dashed lines represent tenfold increments of the system thermal energy. The solid red line represents the energy associated with the saturation velocity of  $1.134\text{\AA}/\text{fs}$ . 25

- FIGURE 3.8: Position as a function of time for ten closed system trajectories with a spread in initial conditions of  $10^{-10}$  for position and velocity. 26
- FIGURE 3.9: Maximal lyapunov exponent across nine trajectories of a closed system. The horizontal dashed line represents the average value which is approximately 23. 27
- FIGURE 3.10: Ten open system trajectories for energy rates of  $10^{-3}$  (left) and 10 (right) in units of thermal energy per picosecond. 28
- FIGURE 3.11: Two sample trajectories with energy exchanges of  $10^{-3}$  (left) and  $10^{-1}$  (right) units of thermal energy per picosecond. The vertical orange lines represent breaking points in orbital behavior. 29
- FIGURE 3.12: Maximal lyapunov exponent across nine trajectories of an open system for each of the five energy rates from  $10^{-3}$  through 10 thermal energy units, each corresponding to a different color (left). Average lyapunov exponent for each energy rate (right). 30
- FIGURE 3.13: Absolute value of the natural log of  $x$ , with  $x$  ranging from  $10^{-10}$  to  $10^{-8}$  and plotted on a log10 axis for ease of viewing. Horizontal black lines represent each energy exchange rate and their respective average lyapunov exponent value. 31
- FIGURE 3.14: Standard deviation in velocity as a function of diffusion coefficient in  $k_B T$  units (left). Log10 of Kurtosis in velocity as a function of diffusion coefficient in  $k_B T$  units (right). Each of the 5 diffusion constants had 10 trajectories and all run velocities were concatenated in order to perform these bulk statistics. 31

## CHAPTER 1: INTRODUCTION

Bohmian mechanics is a deterministic formulation of quantum mechanics that was developed by physicist David Bohm in the 1950s as an alternative to the Copenhagen interpretation of quantum mechanics. In the Copenhagen interpretation, evolution of a system is based on statistical principles such as uncertainty and randomness and suffers from having inconsistencies between the quantum and macroscopic realms involving observations. One of the key features of Bohmian mechanics is that it provides a consistent explanation for the quantum behavior of particles with a smooth transition to classical behavior, while also agreeing with the predictions of the standard interpretation. For example, the theory correctly predicts the outcomes in Young's double-slit experiment, in which a particle passes through two slits and quantum mechanically interferes to produce a characteristic pattern. [1]

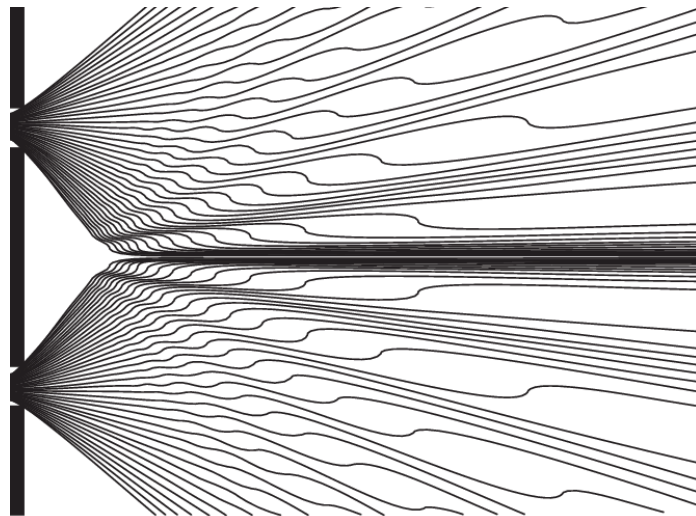


Figure 1.1: Bohmian trajectories for Young's double slit experiment which produce the characteristic interference pattern centered at the midpoint of the two slits. Retrieved from page 57 of [1].

## 1.1 Characterizing Bohmian Mechanics

In Bohmian mechanics, particles are assumed to have definite positions at all times, even when they are not being directly observed. These positions are related to the outcome of a differential velocity field that is dependent on the wave function. The guiding equations from Bohmian mechanics are defined by the following. [2]

$$\frac{dQ}{dt} = \frac{\vec{j}}{|\psi(\vec{r}, t)|^2} \quad (1.1)$$

$$\vec{j} = \frac{\hbar}{m} \Im(\psi(\vec{r}, t)^* \nabla \psi(\vec{r}, t)) \quad (1.2)$$

- $Q$  is the generalized position of a particle.
- $\vec{j}$  is the probability flux.
- $\hbar$  is the reduced Planck constant.
- $m$  is the particle mass.
- $\Im$  represents only the imaginary part of the evaluated function.
- $\psi(\vec{r}, t)^*$  represents the complex conjugate of the wave function.
- $|\psi(\vec{r}, t)|^2$  represents the modulus squared of the wave function.
- $\nabla$  is the vector differential operator, which represents the first derivative of the wave function with respect to position.

## 1.2 Defining Open/Closed Quantum Systems

Open quantum systems are those in which an internal system interacts with an external system. These interactions produce qualities which are vastly different from those of closed systems, which are assumed to be independent of their environment. Characteristics of

closed quantum systems include state coherence, conservation of probability, and unitary evolution.[3] State coherence is characterized by definite phase relationships within the wave function. This is directly related to the superposition principle of quantum mechanics, which is responsible for phenomenon such as entanglement. Probability conservation implies the traditional normalization scheme of the Born interpretation. This ensures that the measured particle is found occupying some state within the total Hilbert space. Unitary evolution means that the dynamics are strictly governed by the Schrödinger equation given by Eq. 1.3. However, any measurement made on a quantum system within the Copenhagen interpretation involves the wave function collapsing, which is a non-unitary process not described the Schrödinger equation. Additionally, the introduction of measuring devices into any system inherently makes them open. This is a major problem for the Copenhagen interpretation that implies true closed systems can never be observed. [4]

$$i\hbar\frac{\partial\psi(\vec{r},t)}{\partial t} = -\frac{\hbar^2}{2m}\nabla^2\psi(\vec{r},t) + V(\vec{r},t)\psi(\vec{r},t) \quad (1.3)$$

- $\psi(\vec{r}, t)$  represents the wave function, which depends on position  $\vec{r}$  and time  $t$ .
- $i$  is the imaginary unit.
- $\frac{\partial}{\partial t}$  represents the partial derivative with respect to time.
- $\frac{\hbar^2}{2m}$  is a constant term related to the kinetic energy of the particle.
- $\nabla^2$  is the Laplacian operator, which represents the second derivative of the wave function with respect to position.
- $V(\vec{r}, t)$  represents the potential energy of the particle, which depends on position  $\vec{r}$  and time  $t$ .

### 1.3 Characterizing Open Quantum Systems

The characteristics of open quantum systems include state decoherence, along with energy, information, and probability fluctuations consistent with system exchanges. State

decoherence is the phenomenon in which phase relationships of state superpositions become unstable through non-unitary operator interactions. This causes quantum systems to exhibit classical behavior due to the partial (or complete) cancellation of the interference term within the superposition calculation. [5] Additionally, fluctuations in observables due to the environment can produce scenarios in which energy, information, or probability are no longer conserved quantities. This phenomenon is commonly referred to as quantum dissipation within the literature. [6] These systems are the quantum analogs to classical systems with irreversible energy loss and the associated Caldeira-Leggett model will be discussed later.

## 1.4 Current Methods of Computing Open Quantum Systems

In the pursuit of understanding and manipulating practical quantum systems, the study of open quantum systems has become increasingly vital. Open systems, interacting with their environment, pose unique challenges and opportunities that demand sophisticated computational approaches for accurate modeling. This section provides an overview of the current methods employed for calculating the dynamics and properties of open quantum systems.

### 1.4.1 Lindblad Model

A popular method for open quantum systems calculations is to use the Lindblad equation. This equation describes the time dynamics of the density matrix, where the rate of change of the density matrix is modified by state jump operators. This equation is Markovian in nature, meaning that it assumes the system-environment interaction to be weak and to have completely uncorrelated system-environment initial conditions. The Markovian condition also imposes that the evolution of the state need not depend on previous states. [7]

$$\dot{\rho} = -\frac{i}{\hbar}[H, \rho] + \sum_i \gamma_i \left( L_i \rho L_i^\dagger - \frac{1}{2} \{L_i^\dagger L_i, \rho\} \right) \quad (1.4)$$

- $\rho$  represents the system's density matrix.

- $H$  represents the system Hamiltonian, describing the unitary aspects of the dynamics.
- $\gamma_i$  are a set of non-negative coefficients called damping rates.
- $L_i$  are a set of jump operators describing the dissipative part of the dynamics.
- $\{a, b\} = ab + ba$  is the anticommutator.

#### 1.4.2 Nakajima-Zwanzig Model

Upon further generalization to open quantum systems of Non-Markovian nature produces the Nakajima-Zwanzig equation. The characteristic feature of this model is its ability to account for previous states, coining the term "quantum memory". It is important to note that what these equations make up for in generality, end up losing greatly in calculability. Solving this equation efficiently often requires many approximations to be employed due to the increased storage demand of saving previous system states. [8][9]

$$\partial_t \rho_S = \mathcal{P} \mathcal{L} \rho_S + \int_0^t dt' \mathcal{K}(t') \rho_S(t - t'). \quad (1.5)$$

- $\rho_S$  represents the system's density matrix.
- $\mathcal{P}$  is the relevant projection operator, such that  $\mathcal{P} + \mathcal{Q} = \mathcal{I}$ .
- $\mathcal{L}$  is a linear operator which always operates from the left on any dynamic variable.
- $\mathcal{K}(t')$  represents the memory kernel, describing the effect of the bath throughout the time evolution of the system.

#### 1.4.3 Caldeira-Leggett Model

Quantum analogs to classical systems with irreversible energy loss are known as dissipative quantum systems and are most commonly associated with the Caldeira-Leggett model. The system-environment coupling is dependent on the type of microscopic system being studied along with the bath. An important requirement is that the bath must have an infinite

number of degrees of freedom to ensure that energy strictly flows out of the system. This condition eliminates the possibility of Poincare recurrences which implies non-ergodicity of the system. Many interesting problems have been studied under a specific realization of this model called the dissipative two-level system. Examples include qubit-environment interactions in quantum computing and quantum phase transitions in condensed matter physics. [10]

$$H = \frac{P^2}{2M} + V(X) + \sum_i \left( \frac{p_i^2}{2m_i} + \frac{1}{2} m_i \omega_i^2 q_i^2 \right) - X \sum_i C_i q_i + X^2 \sum_i \frac{C_i^2}{2m_i \omega_i^2} \quad (1.6)$$

- The first term represents energy through momentum P and mass M.
- V(X) is the potential.
- The third term represents the bath as an infinite sum of harmonic oscillators.
- The fourth term describes the system-bath coupling.
- The last term is a counter which ensures homogeneous dissipation throughout space.

In this approach, one works directly with the wavefunction. However, the wavefunction includes degrees of freedom from the bath making this approach impractical for numerical work on large systems.

#### 1.4.4 Stochastic Bohmian Mechanics Models for Open Quantum System

There are many models which leverage random noise terms to affect quantum system dynamics. Bohm and Vigier [11] included a Wiener stochastic process directly to the velocity from the Bohmian guiding equation.

$$dv = \nabla(V + Q)dt + dW(t) \quad (1.7)$$

- $dv$  represents a small incremental change in velocity.

- $V$  and  $Q$  are the classical potential and quantum potential respectively.
- $dW(t)$  is a random incremental Wiener process.

Another similar approach by Kostin [11] includes a random Gaussian force similar the previous Wiener process but with an added friction term. This equation is consistent, however it only adds incomplete information about a larger system without being fully immersed as the requirement for open quantum systems.

$$i\hbar \frac{\partial \psi(\vec{r}, t)}{\partial t} = -\frac{\hbar^2}{2m} \nabla^2 \psi(\vec{r}, t) + (V(\vec{r}, t) + V_r(\vec{r}, t) + V_D(\vec{r}, t) + G(t))\psi(\vec{r}, t) \quad (1.8)$$

- This is similar to the traditional Schrodinger equation with three added terms.
- $V_r(\vec{r}, t)$  is the random potential.
- $V_D(\vec{r}, t)$  is the damping potential.
- $G(t)$  is a time dependent function based on the average value of  $V_D$  via integration over the position variable.

The advantage of these approaches is that the noise term accounts for the environment with little overhead in cost compared to solving the Bohmian equations of motion for a closed system. However, this formalism is fundamentally inconsistent with quantum mechanics. The calculated momentum (or velocity) should be through Eq.1.1. The random force should influence the velocity, but the way to calculate velocity should fundamentally be through Eq.1.1, which will no longer be valid when a stochastic force is present. This suggest that the stochastic elements of the environment should be through the wavefunction. This observation motivates another approach developed recently by Dr. Jacobs.

### 1.4.5 Modified Schrodinger Equation Approach

A modified Schrodinger equation (MSE) has recently been proposed by Dr. Jacobs, and its framework justifies the approach used here in adding stochastic noise. Since the MSE has not been published yet, a conceptual basis is given, along with some steps describing how the modified Schrodinger equation is developed. While the Schrodinger equation (SE) has been instrumental in describing quantum phenomena, its incompleteness is evident in its failure to model the dynamics of the measurement process.

Dr. Jacobs posits that the Schrodinger Equation (SE) can achieve completeness by linking its latent variables (amplitudes and phases describing the quantum state) to classical degrees of freedom (CDOF) representing environmental effects. This hypothesis introduces a modified Schrodinger equation (MSE) explicitly modeling environmental influences, including the measurement process. Preserving linearity as an extension of the SE, the MSE is solvable through linear differential equations, accommodating non-unitary dynamics while conserving probability. This approach adheres to the postulates of quantum mechanics, producing random outcomes, and representing all observables as Hermitian operators like the Hamiltonian. Notably, it avoids increasing the dimension of the quantum state through direct tensor product representation, hence avoiding partial traces. The "collapse" of the quantum state unfolds continuously, encompassing weak quantum measurements and the Zeno effect as special cases of a context-dependent measurement process.

The incompleteness of the SE becomes evident when solving it for the simplest case of a time-independent Hamiltonian, denoted by  $H_o$ . The formal solution is given as:  $|\psi(t)\rangle = e^{-iHt/\hbar} |\psi(0)\rangle$ . Expanding the initial state vector in the energy basis yields:  $|\psi(t)\rangle = \sum_n R_n e^{-i\phi_n} e^{-iE_n t/\hbar} |n\rangle$ , where  $H_o |n\rangle = E_n |n\rangle$ . This solution (for a system of linear first order differential equations) is unique only if all  $R_n$  and  $\phi_n$  are specified. However, since the quantum system is coupled to its environment (or the process that created its existence at  $t = 0$ ), the influence of the environment will remain present at all times. Therefore, both  $R_n$  and  $\phi_n$  must be functions of time, unless the system is perfectly isolated after  $t = 0^+$ ,

which is when the SE works. For an open quantum system, we must modify the SE to allow  $R_n$  and  $\phi_n$  to depend on time, which creates a communication link between the quantum system dynamics governed by  $H_o$  and CDOF that control the time dependence of  $R_n$  and  $\phi_n$  in a context-dependent manner. Due to the completeness of the vector space spanned by the energy basis, if we specify  $R_n(t)$  and  $\phi_n(t)$ , then it is clear the linear superposition formula given by  $|\psi(t)\rangle = \sum_n R_n(t) e^{-i\phi_n(t)} e^{-iE_n t/\hbar} |n\rangle$  is the proper description of the quantum dynamics.

To obtain the MSE, the first step plugs this general form into the SE, and accounting for the time dependence in  $R_n(t)$  and  $\phi_n(t)$ , more terms are generated, and thus the SE is *not* satisfied. The second step collects these *extra terms*, and after some math and rearrangements, it is found that the Hamiltonian  $H_o$  must be modified to include a noise term, which is called  $H_n(t)$ . This makes the Hamiltonian time dependent, given as:  $H = H_o + H_n(t)$  due to environmental influences. However, additional terms remain that cannot be absorbed into the noise contribution. Collecting these terms, the third step represents them as the ket,  $|\eta(t)\rangle$ . Then the MSE is written as:

$$i\hbar \frac{d}{dt} |\psi\rangle = H |\psi\rangle + i\hbar |\eta\rangle \quad (1.9)$$

Note that  $R_n(t) = \sqrt{P_n(t)}$ , where  $P_n(t)$  is the probability for the quantum system to be in energy state  $n$ . The role that  $|\eta(t)\rangle$  plays is to relate  $\dot{R}_n$  to  $R_n$ . It is remarkable that the quantum system dynamics is determined once  $\dot{R}_n$  is related to  $R_n$  through a constituent equation that defines the *quantum state evolution modulator* given by  $|\eta\rangle$ . There is flexibility in how to construct a constituent equation. For simplicity (and considerable generality), a master equation (ME) can be used such that  $\dot{P}_n(t) = \sum_k \Gamma_{nk} P_k(t)$  and  $\dot{R}_n = \frac{1}{2} \frac{\dot{P}_n(t)}{R_n(t)}$ . where  $\Gamma_{nk}$  are elements of a rate matrix,  $\Gamma$ . Notice that the ME defines a system of linear differential equations (SLDE), and these couple to the original SLDE describing unitary dynamics (from the SE). In short, two SLDE are coupled without increasing the dimension of the quantum state. For the case that  $H_n(t)$  commutes with itself and  $H_o \forall t$ , the MSE can

be solved exactly, presenting no more difficulty than the original SE.

In this thesis, the noise term,  $H_n(t)$  is assumed to commute with itself  $\forall t$  and with  $H_o$ . A Weiner process is applied directly to the phase angle  $\phi_n$ . In this thesis, only the Weiner noise model for  $\phi_n(t)$  is modeled, which is sufficient to demonstrate the effects of an open system. Using a more accurate model will not change the results qualitatively.

### 1.5 Stationary States of Open Quantum Systems

In the literature, certain open quantum systems have been shown to have stationary states coinciding to their closed system counterparts. The derivation surrounding these findings make use of classically open and dissipative systems, in which regular or strange attractors are present. Attractors are subsets of the phase space of dynamical systems. The classification of regular or strange depends on the characteristics of the attractor being studied. Examples include the nonlinear oscillator associated with regular attractors and Lorenz evolution associated with strange attractors. The quantization process involves converting continuous functions of classical mechanics into discrete functions acted on via operators. Utilizing the Lindblad formalism to model the Brownian motion of a quantum harmonic oscillator reveals that the evolution of certain open quantum systems can lead to a unique stationary state that is approached from all initial conditions. [12] [13]

### 1.6 System of Interest: Particle in a Box

The study of a particle in a box represents a quintessential problem in quantum mechanics, serving as a cornerstone in understanding the behavior of spatially confined particles, modelled using an infinite potential well. While the traditional treatment of a particle in a box assumes an isolated system, this study extends the reach of this problem by introducing coupling to an environment. The aim is to describe the interplay between the confined particle and its surrounding environment through quantum trajectories. This study not only broadens our understanding of the foundational principles of quantum mechanics through the Bohmian framework, but also holds relevance in diverse fields, from quantum

information science to condensed matter physics. [14] Through the lens of open quantum systems, the boundaries of the particle in a box problem evolves into a dynamic landscape, offering insights into the balance between coherence and decoherence in quantum systems. Standard eigenfunctions and eigenenergies of the particle in a box are used as a baseline for this study and are defined as the following:

$$\psi_n = \sqrt{\frac{2}{L}} \sin \frac{n\pi x}{L} \quad (1.10)$$

$$E_n = \frac{n^2 h^2}{8mL^2} \quad (1.11)$$

- L is the length of the box.
- n is the quantum number, representing discrete quantum levels.
- h is Planck's constant.
- m is particle mass.

### 1.6.1 Objectives of Study

1. Create a baseline study for the Bohmian mechanics of closed particle in a box systems through the observation of particle initial conditions and trajectories. The following characteristic will be surveyed:
  - Phase effects on initial conditions
  - Positional constraints of the velocity field
  - Lyapunov exponents of phase space trajectories
2. Explore open particle in a box systems by utilizing a diffusive perturbation model where the following characteristics will be investigated:
  - Phase angle diffusion rate
  - Lyapunov exponents of open systems
3. Compare and contrast scaling relationships and system dynamics to identify key differences between system types.
  - Characterize energy profiles of selected diffusion terms
  - Investigate open versus closed Lyapunov exponents
4. Relate findings to practical applications within the quantum realm.

## CHAPTER 2: METHODOLOGY

This section outlines the methodology used to explore open quantum systems within the Bohmian framework. The approach involves modeling the deterministic trajectories of particles influenced by a quantum potential, challenging traditional interpretations. The focus is on capturing interactions, including decoherence and energy exchange, between a quantum system and its environment through diffusive perturbations. By employing this methodology, we aim to unravel the fundamental dynamics of open quantum systems and contribute to the ongoing discussion about determinism in the quantum realm.

### 2.1 Diffusive Processes as Open Quantum System Perturbations

If it is acknowledged that the system is not closed, there must be a surrounding environment. In order to avoid the problem of thermodynamic processes dominating quantum effects, it is assumed that the system and environment are in a state of thermal equilibrium and thus energy may fluctuate between the system and bath. This imposes that the internal energy is not conserved, and it may flow into or out of the system from the environment. Assume the wave function takes the general form of a superposition:

$$\Psi(x, t) = \sum_n R_n e^{-i\phi_n} e^{-iE_n t/\hbar} \psi_n(x) \quad (2.1)$$

- $\Psi(x, t)$  represents the total wave function over all superimposed states.
- $R_n$  represents the magnitude of the expansion coefficient, related to superposition weightings. In closed systems  $R_n$  is a constant. Although  $R_n(t)$  can represent a stochastic process in an open system, for this work  $R_n$  is a constant for closed and open systems determined in the same way.

- $\phi_n$  represents the initial phase angle for the expansion term in a closed system. For an open system,  $\phi$  is a time dependent stochastic variable to model decoherence from the environment.
- $E_n$  represents the energy level for the  $n$ -th non-degenerate state given by:  $E_n = \frac{\hbar^2 \pi^2 n^2}{2mL^2}$ .
- $\psi_n(x)$  represents the energy eigenfunction.

The wavefunction is dynamically altered from the solution to the time-dependent Schrödinger equation due to the effects of the environment on the system when it is open. These dynamical effects occur through stochastic processes that govern the  $R_n$  and  $\phi_n$  time dependence. In general, two separate diffusive processes will take place. The magnitude of the expansion coefficients  $R_n$  fluctuates due to energy exchange with the environment under constant temperature conditions. In principle work can be done on the system through this mechanism because  $R_n^2$  represents the probability of measuring the system with energy  $E_n$ . While the  $R_n$  are characterized by the partition function, they will fluctuate from those ideal values, impacting the weighting within the superposition and thus the probability of the system to have a certain energy.

Similarly, the phase angle given by  $\phi_n$  fluctuates. This change is more subtle, since it relates to a latent variable that cannot be directly measurable, although is critical for outcomes based on superposition. Although both the magnitude and phase can be randomized, this study solely considers phase randomization. This implies that, on average, energy is conserved. Fluctuations in kinetic energy (due to velocity changes) result from phase fluctuations, but phase fluctuations do not alter the average total energy. Therefore, for the systems modeled here, energy fluctuations in kinetic energy are, on average, compensated by the quantum potential. This allows us to compare closed and open systems that differ only by subtle differences in the phase angle, which is a latent variable in the theory of quantum mechanics.

### 2.1.1 Magnitude and Number of Expansion Coefficients

The magnitude of the expansion coefficient for the  $n$ -th energy level is determined as  $R_n = \sqrt{p_n}$ , where  $p_n = \exp(-E_n/k_B T)/Z$  and  $Z = \sum_n^{n_{\max}} \exp(-E_n/k_B T)$ . The number of terms  $n_{\max}$  is adjusted to ensure that the truncation error (resulting from omitting terms with  $n > n_{\max}$ ) remains below 0.001%. This approximation transforms an infinite sum over all quantum numbers into a numerically solvable problem. Note that  $n_{\max}$  increases with particle mass, box size ( $L$ ), or temperature. Based on these limits and expectations of how physical systems respond, and noting the correspondence principle, adding more terms in the expansion is expected to shift the quantum system being modeled towards classical behavior, where quantum effects are less significant. Thus,  $n_{\max}$  plays an important role in describing dynamics while preserving physical relevance, especially considering temperatures below room temperature ( $\approx 300\text{K}$ ). The number of phase terms used in the expansion for the wavefunction, will be explored in this work.

## 2.2 Numerical Scheme for Particle Trajectories

The method behind simulating the quantum trajectories involves a collection of multi-stage MATLAB scripts. The first stage takes user inputs and stores information relevant to the properties of the system to be studied. The second stage is the propagation of the equations of motion. Inputs are passed through a function that creates and evaluates the particle-in-a-box wave functions and necessary derivatives. The expansion across the number of available quantum states is truncated to make calculations accurate on feasible timescales. Analytical formulation of the velocity field through Bohmian mechanics is used in conjunction with the Runge-Kutta integrator at fourth and sixth orders to propagate motion over the entire timescale. In addition to this, stability checks are taken to ensure dynamics are accurately represented. Numerical derivatives of the position are taken to study the quantum potential characteristics of the systems. The third stage involves the storage of the relevant data associated with the system including position, velocity, and

quantum potential profiles. Due to computation time and a large number of simulations, the program was adapted for parallel computation to work within the UNC Charlotte research computing cluster to create a high-throughput pipeline. However, a large number of results were also obtained on a commodity desktop computer.

### 2.3 Quantum Velocity Search Algorithm

The Quantum Velocity Search Algorithm, code named v2phiFinder, is a novel search algorithm that takes a target position and velocity, and outputs the associated set of phases needed to achieve that velocity (within a user controlled tolerance) at that position. This search algorithm functions by iteratively producing a set of new velocities and growing/shrinking the search size depending upon successes/failures. A success is classified as any velocity that is closer in absolute value to the search velocity than the previous best value. After optimizing the number of samples per iteration, tolerance range, and growth/decay constants, almost any velocity can be found at any position when enough phase terms are available for combination (see Chapter 3.1 for more details). Once the phase values are stored from the algorithm, it is possible to recombine them into their respective wave functions to form probability densities or calculate bulk phase statistics.

### 2.4 Calculating Standard Deviation of Phase Sets

A common measure throughout this thesis is standard deviation. However, with the traditional method of numerical computation, order of sets is not important, as is the case for velocity. However, it was quickly observed through clever usage of the Quantum Velocity Search Algorithm, that particular input conditions led to very similar wave functions, and thus had very similar sets of phases as is the case in Figure 3.4. However, when calculating standard deviations of phase sets using the standard treatment, it did not produce the expected values. After careful examination it was found that correct method involved taking the standard deviation along a column, each corresponding to an individual energy eigenfunction, and then taking a final average. Below is an example calculation for a system

with three phase terms per set.

Table 2.1: Table detailing a sample standard deviation calculation for phase sets.

| $n$                   | $\phi_{E_1}$ | $\phi_{E_2}$ | $\phi_{E_3}$ |
|-----------------------|--------------|--------------|--------------|
| Set 1                 | 18.4         | 2.2          | -5.1         |
| Set 2                 | 16.7         | 4.3          | -4.8         |
| Set 3                 | 17.1         | 1.5          | -6.3         |
| Set 4                 | 19.2         | 2.7          | -3.4         |
| $\sigma_{avg} = 1.18$ | 1.16         | 1.19         | 1.19         |

## CHAPTER 3: RESULTS

Exploratory results are presented for quantum trajectories calculated by Bohmian mechanics in both closed and open quantum systems, involving a single particle in a one-dimensional setting. This study marks the first application of the open system model using phase modulation as a stochastic process. Despite its simplicity, this model captures the environmental impact on particle dynamics, offering insights into the dynamic interplay between confined particles and their surroundings.

### 3.1 Closed Systems

With coherence maintained through unitary evolution, closed system results will be shown first as a baseline to make comparisons upon. Since Bohmian mechanics is deterministic in an isolated system, all variation in trajectories derive from differences in the initial conditions. The subsequent dynamics are set for the entirety of the simulation. With this in mind, it is worth pointing out that in classical mechanics, if the initial position and velocity is specified, along with all forces, the trajectories are determined fully. Since the quantum potential creates a quantum force, it is immediately noticed that the specification of the entire wavefunction at  $t = 0$  is part of the initial condition in Bohmian mechanics. This means, the latent variables representing magnitude and phases associated with all the components in the initial quantum state is expected to lead to different trajectories. In the set up used here, the magnitudes of the expansion in energy eigenstates are determined by the Boltzmann weights, as described above. Only the initial phases are being randomly generated.

### 3.1.1 Single Point Evaluation

The purpose of this section is to highlight the velocity profile across a series of observations at a singular irrational position  $a_x/\sqrt{2}$ . The reason why an irrational point was selected is because an effort was made not to fall on a position where one of the eigenstate functions had a node at that point. This concern appears not important provided the initial point is not  $a_x/2$  and if the number of expansion terms is large. In this case, for an electron and box length of 100 Å, the results shown here are typical. For each observation, the set of phases within the superposition of states are randomized in a controlled manner according to the standard deviation  $\sigma_\phi$  of a Gaussian distribution centered at zero. Each set of phases corresponds to a different probability distribution and velocity field, thus it is possible to observe the deviation in mean and standard deviation in the velocity measurements as  $\sigma_\phi$  is varied.

The four panel graphic in Fig 3.1 highlights  $\sigma_\phi$  increasing in tenfold increments. At first, the velocity profile is localized to the region surrounding this particular zero phase velocity value (0.199 Å/fs). However, as  $\sigma_\phi$  is increased further, the mean velocity value shifts to zero and the standard deviation saturates at a value of roughly 2. As the phase values become more randomized about  $2\pi$ , it is possible for the velocity to have positive or negative values due to the larger variation in initial conditions. The result of mean shifting is in agreement with the classical limit, as any classical particle may have an initial condition moving one direction (small  $\sigma_\phi$  representing low sampling), but will eventually change directions after contacting the wall (large  $\sigma_\phi$  representing higher sampling).

In order to understand the nature of these distributions, another set of observations was made to calculate the standard deviation and kurtosis of the associated velocity initial conditions as a function of sample number. The reasoning behind this was to test for saturation in either value to give a relative understanding of which statistical moments have bounds. The standard deviation is related to the second statistical moment, while kurtosis is related to the fourth statistical moment.

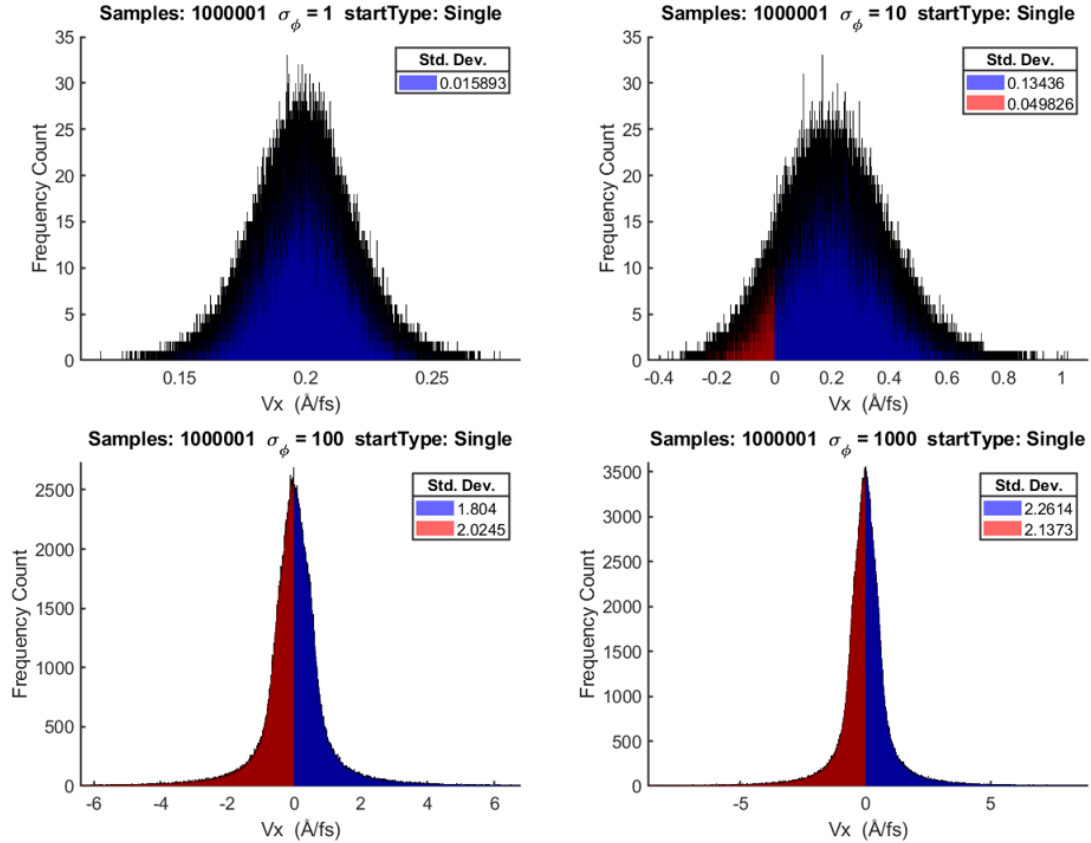


Figure 3.1: Frequency count of velocities generated as initial conditions with  $\sigma_\phi$  increasing in tenfold increments. Red represents negative velocity values, blue represents positive. The standard deviation of velocity is given in the top right of each graph.

The average value for standard deviation levels off as a function of samples, while mean kurtosis continues to increase exponentially. Thus, it can be concluded that the second moment of the velocity distribution exists as some bounded number, while the fourth moment does not. This allows for the elimination of many traditional types of distributions including that of Gaussian or Laplacian nature and helps in characterizing that the distribution is highly heavy-tailed, which is also evident based on the presence of extreme values in the data sets.

### 3.1.2 Linear Evaluation

The purpose of this section is to highlight velocity and phase profiles across a series of observations in a linear set of positions across the length of the box. This systematic

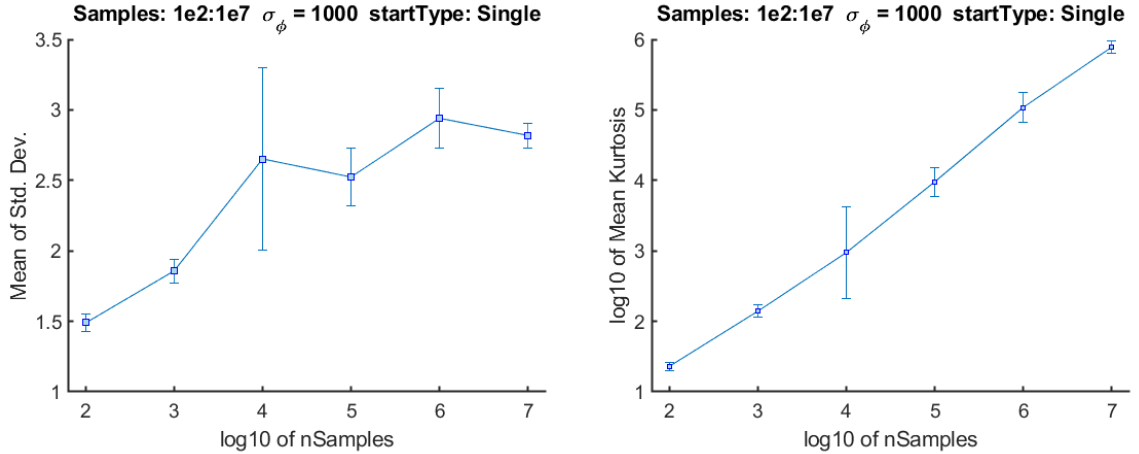


Figure 3.2: The mean of standard deviations as a function of  $\log_{10}$  of samples (left) shows each mean value with a small square box and vertical error bars. The mean of  $\log_{10}$  of kurtosis as a function of  $\log_{10}$  of samples (right) shows each mean value with a small square box and vertical error bars.

sweep over positions will reveal a relationship between the standard deviation in phase and its effect upon velocity. This relationship will allow for the creation of phase diffusion coefficients with physical ties which can be used in the open system analysis later.

In order to start this analysis, box size and velocity must be studied for any effects on phase. The initial interest in this study arose from data suggesting that for a box size of  $100\text{\AA}$ , that only certain velocities could be found by the quantum velocity search algorithm when the position was near the center point  $a_x/2$ . Thus, two more box sizes were observed and it was found that similar results existed to a larger degree in the  $50\text{\AA}$  case, but not observed at all in the case of  $200\text{\AA}$ . The apparent failure of the algorithm can be seen as the dark blue areas in each graph of Fig. 3.3, highlighting that the center of the box is a problematic point once the search velocity is increased. Actually, it is not the algorithm that fails, but rather, the center of the box appears to represent a pathological point. However, as more terms in the expansion over energy eigenstates is considered, the maximum speed increases. More terms can be generated by increasing temperature, increasing mass or increasing the linear dimensions of the box. All three trends tend to bring us from the

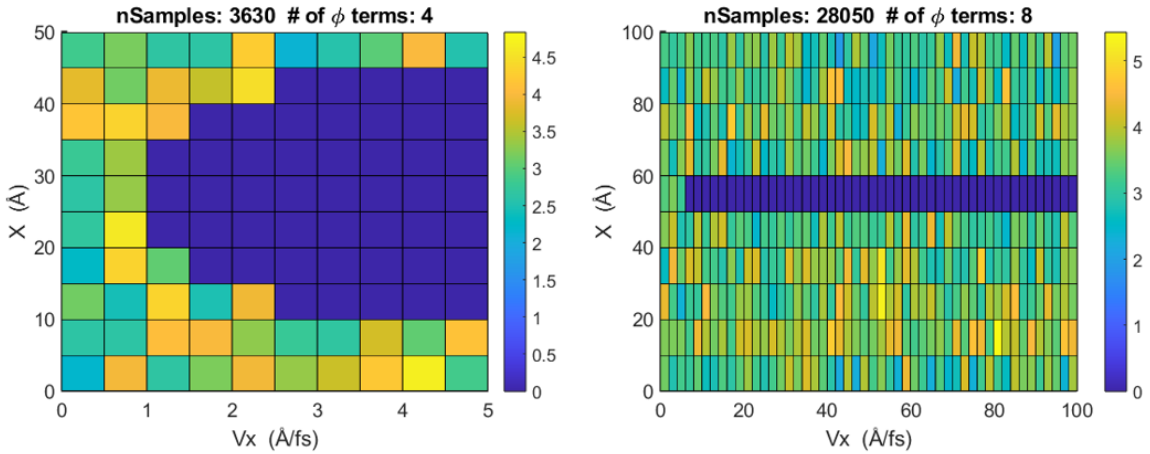


Figure 3.3: Surface plots highlighting position and velocity as inputs for the search algorithm which outputs phases for box sizes of  $50\text{\AA}$  (left) and  $100\text{\AA}$  (right). The standard deviation of each set of phases are represented as colors along the grid. The color bar is a legend showing the range of values and the corresponding colors.

quantum to classical regime.

The phase randomization algorithm produces the intended velocity (within a specified tolerance) at any designated position (if within the allowable range of velocities). It is found that there is a significant degeneracy in wavefunctions that results in identical classical initial conditions. This degeneracy is characterized by the standard deviation in the phases. Once these phases are determined to set the initial conditions, the initial probability density from the wave function can be determined. This is done to qualitatively observe how the shape of the probability density changes as the initial speed of the particle is increased.

As the search velocity is increased, it is observed that there is an overall convergence in the probability densities compared to low search velocities. This fact points to the conclusion that integer divisions of the box length and their range of searchable velocities heavily coincide to the relative number of phase terms that the algorithm is able to target. This explains why the non-searchable region became larger when the box size decreased, due to the number of phase terms decreasing as well. The inverse of the previous statement also explains why when the box size was increased to  $200\text{\AA}$ , that the non-searchable region

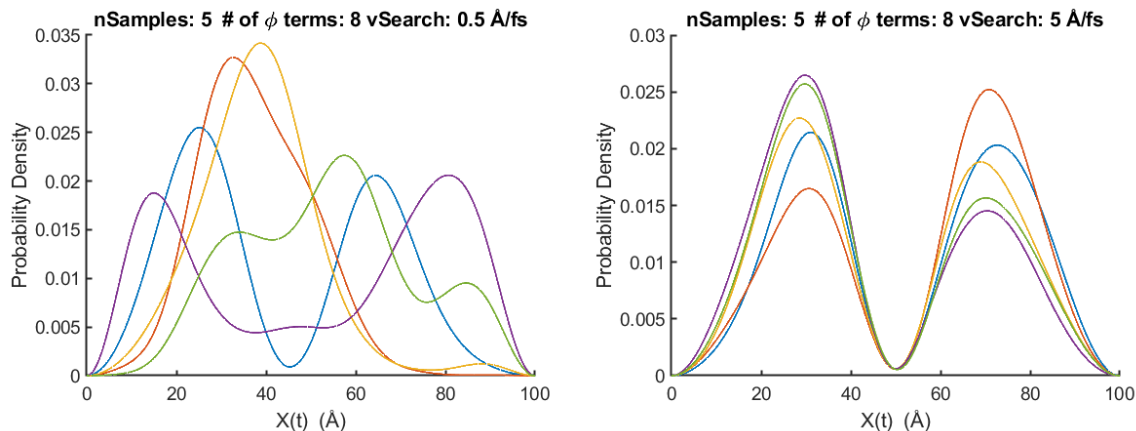


Figure 3.4: Sets of 5 probability densities generated from initial conditions with box size of  $100\text{\AA}$  and search velocities of  $0.5\text{\AA}/\text{fs}$  (left) and  $5\text{\AA}/\text{fs}$  (right).

vanished due to the increase in phase terms as seen in Fig. 3.5.

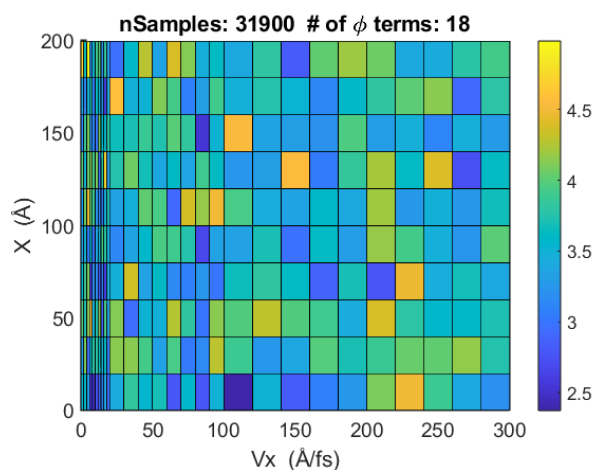


Figure 3.5: Surface plot highlighting position and velocity as inputs for the search algorithm which outputs phases for a box size of  $200\text{\AA}$ . The standard deviation of each set of phases are represented as colors along the grid. The color bar is a legend showing the range of values and the corresponding colors.

## 3.2 Open Systems

The characterization of closed systems in section 3.1 was a preliminary step for understanding the system parameters used in this open system study. Leveraging the knowledge of positional constraints and the connection with phase terms, this study will be conducted with a box length of  $200\text{\AA}$ . The goal of this section is to make a series of qualitative and quantitative comparisons across multiple phase diffusion coefficients, which will be related to the thermal energy of the system.

### 3.2.1 Phase to Energy Relationship

In order to relate the diffusion coefficient of phases to energy exchange in the system, the standard deviation in velocity must be tied to the standard deviation in phases. Once this relationship is solidified, an effective kinetic energy  $\frac{1}{2}m\sigma_v^2$  can be associated with a saturation value located at the median standard deviation in velocity  $\sigma_{vM}$ . Finally, the effective kinetic energy rate can be related to the thermal energy  $k_bT$  of the system and used to estimate the needed coefficient to produce that amount of energy change per picosecond.

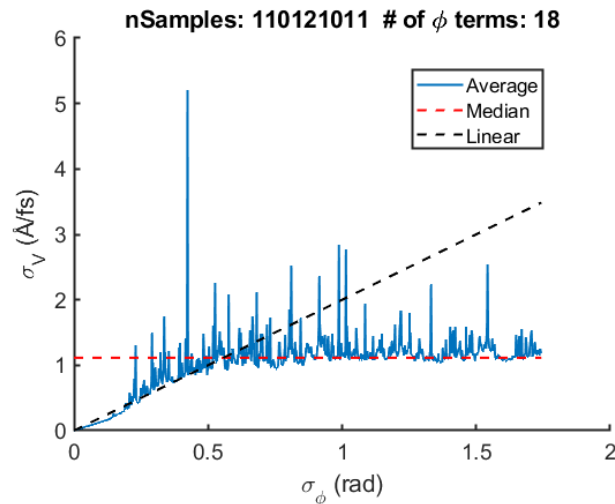


Figure 3.6: Average standard deviation of velocity as a function of standard deviation of phases (solid blue). A linear fit (black dashed line) with a slope of  $2\text{\AA}/(\text{fs rad})$  is fitted to the initial portion (approximately  $0.55\text{ rad}$ ) until saturation is met, represented by the median value of  $1.134\text{\AA}/\text{fs}$  (red dashed line).

The data in Figure 3.6 is averaged from a linear spacing across the 200Å box, for a series of randomized sets of phases controlled by  $\sigma_\phi$ , leading to over 110 million samples included. The median value is used as a saturation point in scaling, representing the point of maximal phase influence. The large spikes in this graph are an intrinsic effect of the system due to the heavy tails of the velocity distribution as stated earlier. The velocities from the linear fit in Figure 3.6 are transformed into energies via  $\frac{1}{2}m\sigma_v^2$ . This relationship is most easily viewed as a log-log plot when working in tenfold increments of the system thermal energy (about 0.026 eV) as seen in Figure 3.7. The x value of intercepts between the blue dashed lines with the linear black line can be used to give the required spreading in phase corresponding to that many units of system thermal energy, ranging from  $10^{-3}$  to  $10$ .

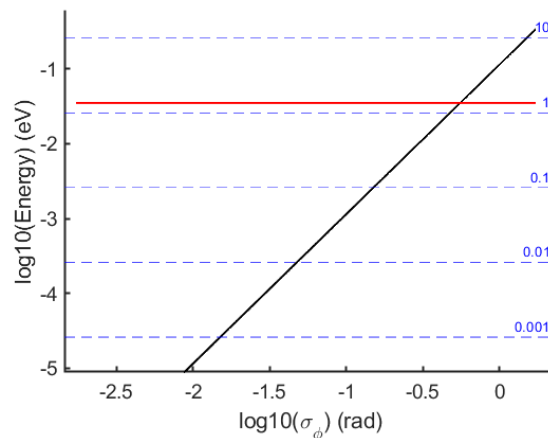


Figure 3.7: Log-Log plot of Energy Rate as a function of standard deviation of phase (solid black). The horizontal dashed lines represent tenfold increments of the system thermal energy. The solid red line represents the energy associated with the saturation velocity of 1.134Å/fs.

### 3.2.2 Trajectory Analysis

A total of five cases will be presented in this trajectory analysis with phase diffusion rates corresponding to  $10^{-3}$  through  $10^1$  thermal energy units. The analysis will consist of lyapunov exponent calculations and a qualitative counting of orbit changes. All of the following comparisons will be made with the closed system equivalent as a baseline.

Additionally, to produce lyapunov exponents, a spread size of  $10^{-10}$  is used to generate each initial condition set of position and velocity. These sets of initial conditions are then used as inputs for the quantum velocity search algorithm to produce the starting wave function for each trajectory. The following formula is used as the basis for calculating lyapunov exponents in this analysis.

$$\lambda = \lim_{t \rightarrow \infty} \lim_{|\delta \mathbf{Z}_0| \rightarrow 0} \frac{1}{t} \ln \frac{|\delta \mathbf{Z}(t)|}{|\delta \mathbf{Z}_0|} \quad (3.1)$$

- $\lambda$  represents the lyapunov exponent.
- $|\delta \mathbf{Z}(t)|$  represents the absolute change over any two trajectories.
- $|\delta \mathbf{Z}_0|$  represents the initial separation between trajectories.
- The limit that  $|\delta \mathbf{Z}_0| \rightarrow 0$  ensures validity of the linear approximation. [15]
- Positive lyapunov exponents typically correspond to chaotic systems.

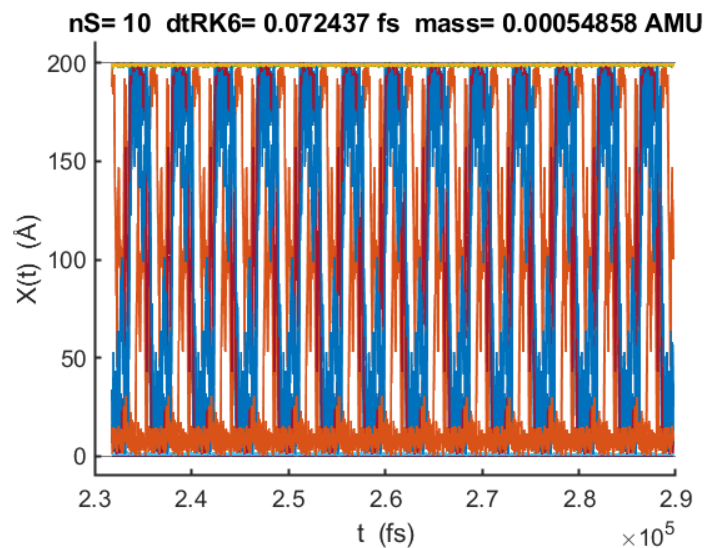


Figure 3.8: Position as a function of time for ten closed system trajectories with a spread in initial conditions of  $10^{-10}$  for position and velocity.

The closed system trajectories in Figure 3.8 are well beyond the time of transient behavior and are shown in their steady state orbits. Of the ten trajectories overlaid, some have orbits spanning the length of the box, and others are strictly positioned to one side or the other. The Lyapunov exponent calculation for this specific case gives an average value of approximately 23, pointing to the conclusion that these trajectories are part of a system with the presence of chaotic attractors.

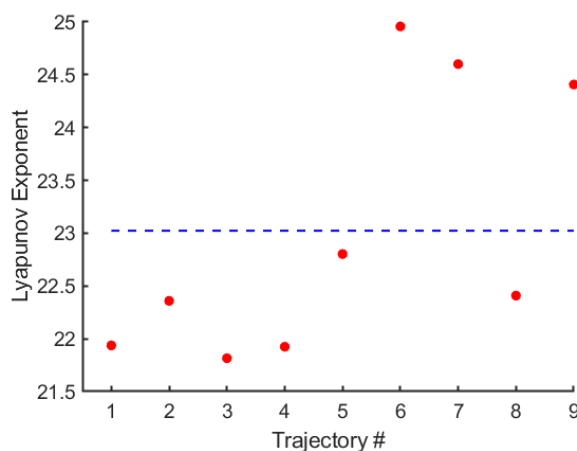


Figure 3.9: Maximal Lyapunov exponent across nine trajectories of a closed system. The horizontal dashed line represents the average value which is approximately 23.

Now that the closed system has been characterized, the analysis on the open system trajectories can be compared. The trajectories in Figure 3.10 can be seen with no repeating orbits, whereas the closed system in Figure 3.8 had only stable orbits. Additionally, the case representing an energy rate of  $10^{-3}$  thermal units (3.10 Left) has a trajectory profile closely matching that of the closed system, with the addition of instability of orbits. However, the case representing 10 thermal units of energy exchange per picosecond is much more random, showing little orbital behavior (3.10 Right).

In Figure 3.11 it is observed that as the orbits decrease stability as the energy exchange constant is increased. The left panel shows a case of  $10^{-3}$  units of thermal energy per

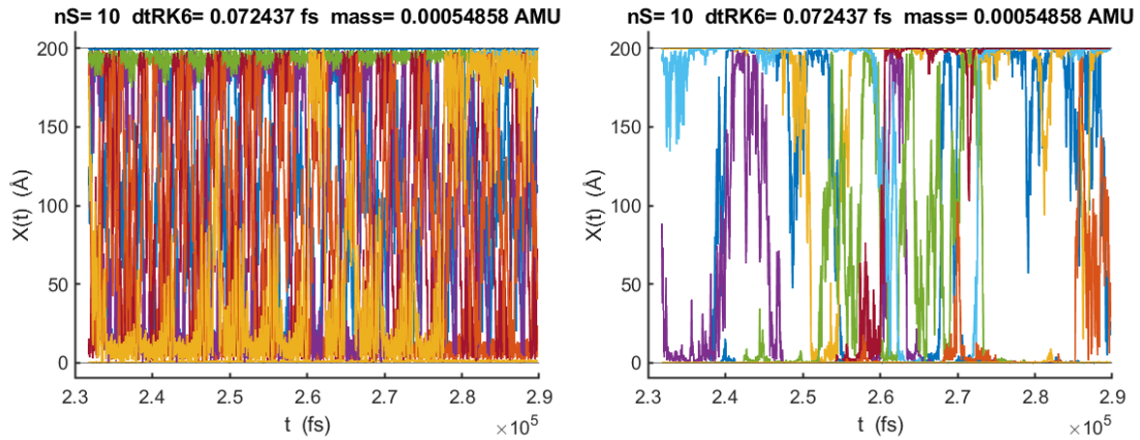


Figure 3.10: Ten open system trajectories for energy rates of  $10^{-3}$  (left) and 10 (right) in units of thermal energy per picosecond.

picosecond, with only 4 regions. The right panel shows a case of  $10^{-1}$  units of thermal energy per picosecond with 8 distinct regions. Therefore, the average time per region decreased by half when the energy exchange rate was increased by a hundred times. This halving effect persists in higher energy systems, leaving room for little orbital detection, thus making the trajectories seem mostly random. Another interesting feature of Figure 3.11 (left) is a intermediate orbital between the third and fourth regions, highlighting the ability for phase perturbations to give way to smooth transitions under the correct conditions.

In Figure 3.12 (right), it is observed that the average value from all open system runs decreased as a function of the energy exchange rate, and is below the average produced by the closed system (approximately 23). One can argue that these diffusive phase perturbations are causing a disruption to the strength of the phase-space attractors. This is also observed by qualitatively comparing the trajectories in Figures 3.8 (closed) to 3.10 (open).

Observation of the general form for maximal lyapunov exponent in Equation 3.1 shows the presence of a natural logarithm. When comparing the average values of both open and closed systems, it is clear that the closed system directly corresponds to the spread

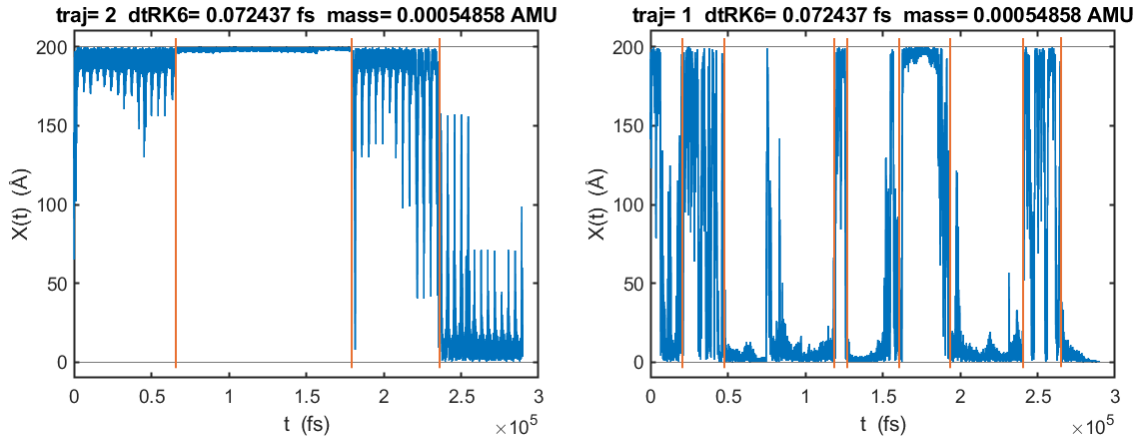


Figure 3.11: Two sample trajectories with energy exchanges of  $10^{-3}$  (left) and  $10^{-1}$  (right) units of thermal energy per picosecond. The vertical orange lines represent breaking points in orbital behavior.

size of  $10^{-10}$ , defined earlier as the initial allowed deviation for both position and velocity. However, the open systems align with spread values ranging from  $10^{-9.5}$  to  $10^{-8.25}$ . For this specific set of initial conditions, opening the system corresponds to same effect as increasing the initial spread of initial conditions by  $10^{0.5}$  to  $10^{1.75}$ , depending on the energy exchange rate used, for both position and velocity in the lyapunov analysis.

Analyzing the velocity distribution across the open system trajectories revealed that the standard deviation in velocity decreased as a function of diffusion rate. However, the decreasing trend saturated at an exchange rate of 1 unit of thermal energy. A decrease in standard deviation over the entire set of trajectories supports the previous statements about the open system disruption of orbits, due to the largest contributions coming from that of stable orbits across the entire length of the box. This conclusion is supported by the data from 3.10 which clearly shows the disturbance of cross box orbits as the thermal exchange rate is increased. Additionally, the kurtosis saw an increase from Figure  $\sim 10^2$  (closed) to  $\sim 10^4$  through  $10^6$  (open) depending on the diffusion rate. Overall, these relationships show that the velocity distributions become sharper with wider tails as the diffusion rate is increased. However, this does not point to the conclusion that open system dynamics are

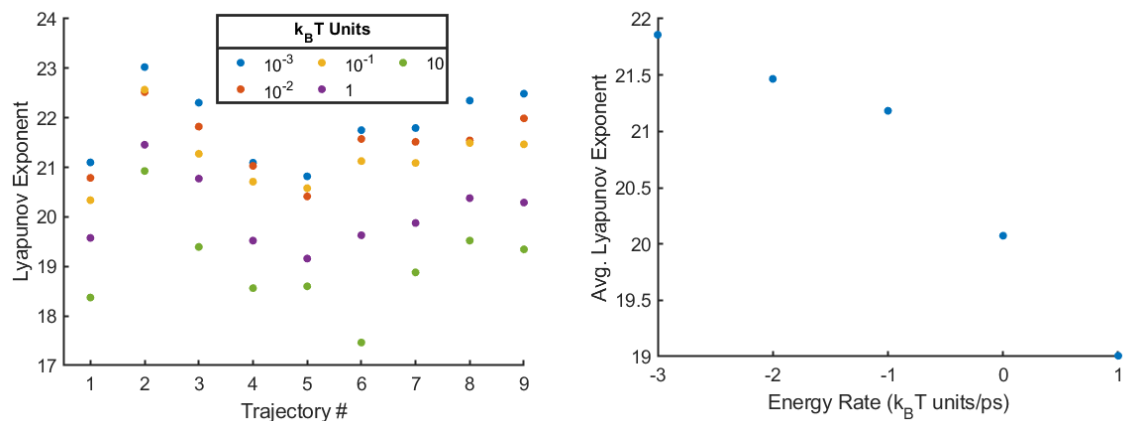


Figure 3.12: Maximal lyapunov exponent across nine trajectories of an open system for each of the five energy rates from  $10^{-3}$  through 10 thermal energy units, each corresponding to a different color (left). Average lyapunov exponent for each energy rate (right).

more classical appearing than their closed counterparts.

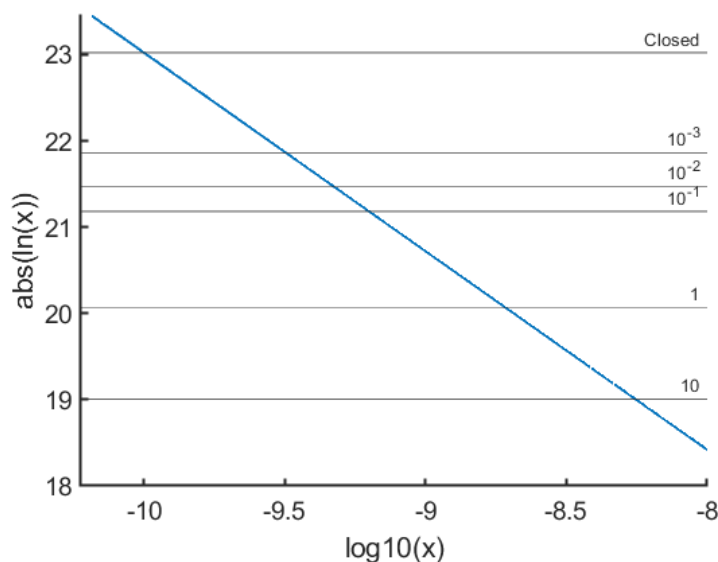


Figure 3.13: Absolute value of the natural log of  $x$ , with  $x$  ranging from  $10^{-10}$  to  $10^{-8}$  and plotted on a  $\log_{10}$  axis for ease of viewing. Horizontal black lines represent each energy exchange rate and their respective average lyapunov exponent value.

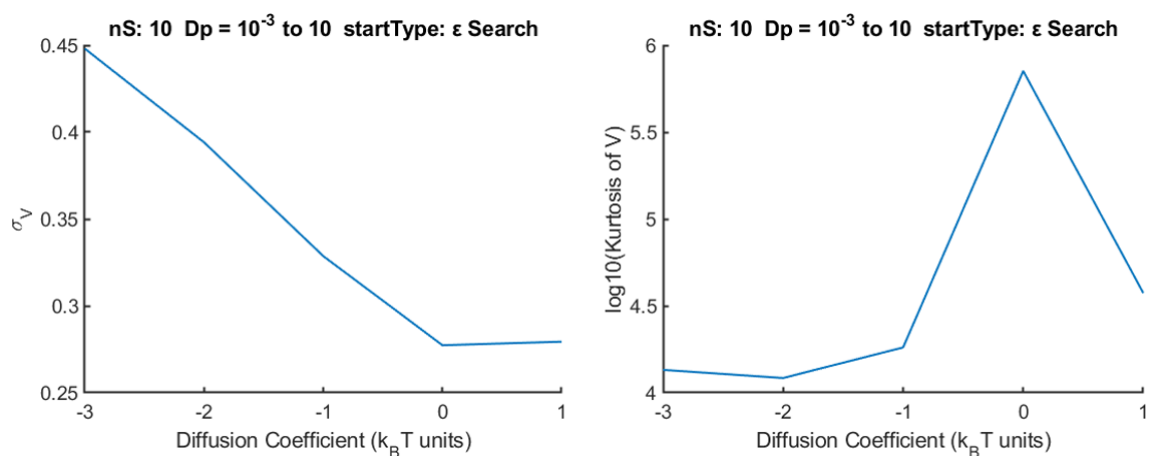


Figure 3.14: Standard deviation in velocity as a function of diffusion coefficient in  $k_B T$  units (left).  $\log_{10}$  of Kurtosis in velocity as a function of diffusion coefficient in  $k_B T$  units (right). Each of the 5 diffusion constants had 10 trajectories and all run velocities were concatenated in order to perform these bulk statistics.

## CHAPTER 4: CONCLUSION

In conclusion, this thesis has directly advanced the understanding of quantum phases and the relationship they share with particle trajectories in both closed and open Bohmian systems. Creation of the Quantum Velocity Search Algorithm, an inverse search method that can output sets of quantum phases (allowing for wave function reconstruction) given position and velocity information, was instrumental in the results produced in this thesis. Meticulous analysis of closed systems led to a variety of results, the most important of which are the velocity distribution characteristics and positional velocity constraints. The total number of phase terms had a drastic effect on the distribution of velocity constraints, as sets of 4 phases could only produce speeds of  $1\text{\AA}/\text{fs}$  at the center of the box, while sets of 18 could produce speeds even up to a tenth of the speed of light ( $300\text{\AA}/\text{fs}$ ). The open system analysis heavily relied on information gathered from the closed system and allowed for the scale of phase diffusion coefficients to be tied to thermal energy units of the system. Qualitative comparisons were made across closed and open systems, along with quantitative measures such as maximal lyapunov exponents. All of which point to the conclusion that open systems heavily disrupt closed quantum behavior. The point of scaling saturation for the phase diffusion coefficient is directly associated to the fact that phases are bound to the unit circle and values above or below  $[0, 2\pi]$  simply repeat. This fact means that the energy produced through phase perturbations has a maximal rate around 1 unit of system thermal energy per picosecond. Overall, this thesis paves the way for future analysis on open quantum systems using the Bohmian framework and acts to further blur the lines between determinism and indeterminism in the quantum world.

## REFERENCES

- [1] D. Dürr, S. Goldstein, R. Tumulka, and N. Zanghí, “Bohmian mechanics,” in *Compendium of quantum physics*, pp. 47–55, Springer, 2009.
- [2] D. Bohm, “A suggested interpretation of the quantum theory in terms of “hidden” variables. i,” vol. 85, p. 166, APS, 1952.
- [3] J. B. Hartle, “The quantum mechanics of closed systems,” *arXiv preprint gr-qc/9210006*, 1992.
- [4] M. Schlosshauer, “Decoherence, the measurement problem, and interpretations of quantum mechanics,” *Reviews of Modern physics*, vol. 76, no. 4, p. 1267, 2005.
- [5] W. H. Zurek, “Decoherence, einselection, and the quantum origins of the classical,” *Reviews of modern physics*, vol. 75, no. 3, p. 715, 2003.
- [6] E. Celeghini, M. Rasetti, and G. Vitiello, “Quantum dissipation,” *Annals of Physics*, vol. 215, no. 1, pp. 156–170, 1992.
- [7] D. Manzano, “A short introduction to the lindblad master equation,” *Aip Advances*, vol. 10, no. 2, 2020.
- [8] S. Nakajima, “On quantum theory of transport phenomena: steady diffusion,” *Progress of Theoretical Physics*, vol. 20, no. 6, pp. 948–959, 1958.
- [9] R. Zwanzig, “Ensemble method in the theory of irreversibility,” *The Journal of Chemical Physics*, vol. 33, no. 5, pp. 1338–1341, 1960.
- [10] A. O. Caldeira and A. J. Leggett, “Influence of dissipation on quantum tunneling in macroscopic systems,” *Physical Review Letters*, vol. 46, no. 4, p. 211, 1981.
- [11] A. B. Nassar and S. Miret-Artés, “Bohmian mechanics, open quantum systems and continuous measurements,” 2017.
- [12] V. E. Tarasov, “Pure stationary states of open quantum systems,” *Physical Review E*, vol. 66, no. 5, p. 056116, 2002.
- [13] V. E. Tarasov, “Classical canonical distribution for dissipative systems,” *Modern Physics Letters B*, vol. 17, no. 23, pp. 1219–1226, 2003.
- [14] A. Onyia, H. Ikeri, and A. Nwobodo, “Theoretical study of the quantum confinement effects on quantum dots using particle in a box model,” *Journal of Ovonic Research*, vol. 14, no. 1, pp. 49–54, 2018.
- [15] A. Vulpiani, F. Cecconi, and M. Cencini, *Chaos: from simple models to complex systems*, vol. 17. World Scientific, 2009.